Title
Advanced Differential Approximation Formulation of the PN Method for Radiative Transfer

Journal
Journal of Heat Transfer, 137(7)

ISSN
0022-1481

Authors
Pal, Gopalendu
Modest, Michael F

Publication Date
2015-07-01

DOI
10.1115/1.4029814

Peer reviewed

Advanced Differential Approximation Formulation of the P_N Method for Radiative Transfer

Gopalendu Pal
CD-Adapco,
Lebanon, NH 03766
e-mail: gopalendu.pal@cd-adapco.com

Michael F. Modest
School of Engineering,
University of California,
Merced, CA 95343
e-mail: mmodest@eng.ucmerced.edu

The spherical harmonics (P_N) method, especially its lowest order, i.e., the P_1 or differential approximation, enjoys great popularity because of its relative simplicity and compatibility with standard models for the solution of the (overall) energy equation. Low-order P_N approximations perform poorly in the presence of strongly nonisotropic intensity distributions, especially in optically thin situations within nonisothermal enclosures (due to variation in surface radiosities across the enclosure surface, causing rapid change of irradiation over incoming directions). A previous modification of the P_N approximation, i.e., the modified differential approximation (MDA), separates wall emission from medium emission to reduce the nonisotropy of intensity. Although successful, the major drawback of this method is that the intensity at the walls is set to zero into outward directions, while incoming intensity is nonzero, resulting in a discontinuity at grazing angles. To alleviate this problem, a new approach, termed here the "advanced differential approximation (ADA)," is developed, in which the directional gradient of the intensity at the wall is minimized. This makes the intensity distribution continuous for the P_1 method and mostly continuous for higher-order P_N methods. The new method is tested for a 1D slab and concentric spheres and for a 2D medium. Results are compared with the exact analytical solutions for the 1D slab as well as the Monte Carlo-based simulations for 2D media. [DOI: 10.1115/1.4029814]

Keywords: advanced differential approximation, heat transfer, radiative transfer equation, spherical harmonics method

Introduction

The radiation transport equation (RTE) is an integro-differential equation for the radiative intensity in five independent variables (three space coordinates and two direction coordinates). One more layer of complexity is added due to the nongray (wavelength dependent) nature of the participating medium. Similarly, the presence of other modes of heat transfer makes the problem more complex, because intensity is coupled to the source term of the overall energy conservation equation in a nonlinear manner. Exact analytical solutions to the equation of radiative transfer are exceedingly difficult to obtain and explicit solutions are only possible for very simple situations, such as one-dimensional plane-parallel media without scattering. For more complicated problems involving multidimensional irregular geometry, anisotropic scattering, or inhomogeneous media, several approximate methods have been developed over time. Among these, the most popular methods are [1]: (1) spherical harmonics method (SHM), (2) discrete ordinate method (DOM) or finite volume method (FVM), (3) zonal method, and (4) Monte Carlo method. While the first three are deterministic in nature, the fourth one is a statistical method.

Statistical methods like the Monte Carlo method can solve the most complicated problems with relative ease, but they are always subject to statistical error and require great computational cost. The zonal method enjoyed initial popularity but is rarely used today due to its great computational expense requiring inversion of full matrices and inability to treat anisotropic scattering. Hence, out of the three deterministic methods, SHM and DOM have received the most attention and have been developed over the years. In both these methods, the RTE is simplified to sets of spatial differential equations by approximating the directional dependence of intensity. The difference between SHM and DOM is how the directional dependence of the radiative intensity is approximated. The DOM discretizes the directional variation using numerical quadrature for integrals over the total solid angle 4π. Thus, DOM is basically an application of the finite difference or finite volume (when discretization is applied using solid angle volumes) scheme over the RTE. Despite the simplicity and methodical development of DOM, it suffers from several drawbacks, such as ray effects, false scattering due to its angular discretization [2], requirement of iterative solutions in the presence of scattering media or reflecting surfaces, and slow convergence in optically thick media.

The SHM captures the directional distribution of intensity by expressing it into a series of orthogonal spherical harmonics. Various orders of accuracy can be obtained by truncating the series after the desired number of terms [1]. The SHM has several advantages over other approximate methods: (1) The relatively simple partial differential equations reduced from the RTE can be solved using standard PDE solver packages, making it easy to implement using standard flow solver data structures; (2) the SHM is a spectral method, it requires fewer terms than DOM for similar accuracy; (3) unlike DOM/FVM, CPU time requirements for SHM do not increase for scattering media and reflecting walls, nor for optically thick media. The lowest-order P_N approximation, the P_1 method has so far been the most popular RTE solver within the SHM framework because of its simplicity [1]. But its accuracy is questionable in the presence of strong directional gradients in intensity. To achieve a higher order of accuracy, a number of higher-order P_N approximations have been formulated for specific geometries by exploiting the symmetry of the media [3–7]. The three-dimensional P_N approximation for arbitrary coordinate

Contributed by the Heat Transfer Division of ASME for publication in the JOURNAL OF HEAT TRANSFER. Manuscript received August 13, 2013; final manuscript received February 2, 2015; published online March 24, 2015. Assoc. Editor: Zhuomin Zhang.

systems was derived by Ou and Liou [8], formulating a set of $(N+1)^2$ complex, coupled, first-order PDEs similar to DOM, without, however, discussing boundary conditions. Recently, Yang and Modest formulated a generic methodology that decomposes the RTE into $N(N+1)/2$ coupled, second-order elliptic partial differential equations for a given odd order N, allowing for variable properties and arbitrary three-dimensional geometries, including a set of generic boundary conditions [9].

The mathematical complexity increases rapidly if higher-order P_N approximations for multidimensional geometry are desired, which is probably responsible for the fact that its development lags behind that of the DOM/FVM. The fact that in the SHM intensity is expressed in terms of a series of spherical harmonics makes it difficult to accurately represent directionally strongly anisotropic intensity, as encountered, for example, near emitting walls and/or in optically thin media. To alleviate this problem for P_1, several strategies have been developed, such as the MDA [10–13] and the improved differential approximation [14–16]. Recently, Yang and Modest showed that the MDA approach can be applied to all orders of P_N, making it more accurate by separating wall emission from medium emission to reduce the nonisotropy of intensity [17]. Although somewhat successful, the major drawback of this method remains that the intensity at the walls is set to zero for outward directions, while incoming intensity is nonzero, resulting in a discontinuity at grazing angles, which cannot be represented accurately by a series of spherical harmonics.

This article discusses the development of a new approach, termed here the ADA. The intensity is broken up into two parts—one is related to the wall emission and the other to a combination of wall and medium emission in such a way as to minimize wall intensity discontinuity at the grazing angles. Detailed mathematical development of the ADA is provided in this paper with a discussion of the differences between the ADA and the MDA approaches. The new method is tested for a 1D slab and concentric spheres, and for a 2D medium. The ADA results are compared with exact analytical solutions, the ordinary differential approximation (ODA) and the MDA results for 1D media. For the 2D media, the ADA results are compared with those from the traditional P_N methods (i.e., the ODA), the MDA method, and the Monte Carlo method.

Mathematical Development of ADA

Although the ADA can be applied to the general radiative transfer equation (RTE), for brevity and clarity of the mathematical formulation, here the development of the ADA is shown for an isotropically scattering medium. Consider an arbitrary enclosure containing an emitting–absorbing–scattering medium. The RTE for a medium on a spectral/gray basis reduces to [1]

$$\frac{\mathrm{d}I}{\mathrm{d}s} = \kappa I_\mathrm{b} - \beta I + \frac{\sigma_\mathrm{s}}{4\pi}\int_{4\pi} I(\hat{s}')\Phi(\hat{s},\hat{s}')d\Omega' \tag{1}$$

Here, I is the radiative intensity, κ the absorption coefficient, σ_s the scattering coefficient, β the extinction coefficient $(=\kappa+\sigma_\mathrm{s})$, and I_b the blackbody intensity; $\hat{s}$ is a unit direction vector, Φ is the scattering phase function, and Ω the solid angle.

For isotropic scattering, i.e., $\Phi(\hat{s},\hat{s}')=1$, the RTE (1) can be written as

$$\frac{1}{\beta}\frac{\mathrm{d}I}{\mathrm{d}s} = (1-\omega)I_\mathrm{b} - I + \frac{\omega}{4\pi}G \tag{2}$$

where ω is the scattering albedo $(=\sigma_\mathrm{s}/\beta)$ and G the incident radiation $\left(=\int_{4\pi} I(\hat{s}')d\Omega'\right)$.

For diffusely reflecting walls, Eq. (2) is subject to the boundary condition [1]

$$I(\mathbf{r}_\mathbf{w},\hat{\mathbf{s}}) = \frac{J_\mathrm{w}}{\pi}(\mathbf{r}_\mathbf{w}) = I_\mathrm{bw}(\mathbf{r}_\mathbf{w}) - \frac{1-\epsilon}{\pi\epsilon}\mathbf{q}\cdot\hat{\mathbf{n}}(\mathbf{r}_\mathbf{w}) \tag{3}$$

where J_w is the total surface radiosity, and ϵ is the surface emittance.

Similar to the MDA [1], the intensity at any point will be broken up into two components: one, I_w, which may be traced back to emission from the enclosure wall but may have been attenuated by absorption and scattering in the medium and by reflection from the enclosure walls; and the remainder I_m, which may be traced back to radiative intensity released within the medium into a given direction by scattering and absorption. However, in contrast to MDA, part of I_m may be due to (possibly negative) wall emission. Thus

$$I(\mathbf{r},\hat{\mathbf{s}}) = I_\mathrm{w}(\mathbf{r},\hat{\mathbf{s}}) + I_\mathrm{m}(\mathbf{r},\hat{\mathbf{s}}) \tag{4}$$

The RTE in Eq. (2) can also be broken into two parts, such that I_w satisfies the equation

$$\frac{\mathrm{d}I_\mathrm{w}}{\mathrm{d}\tau_\mathrm{s}}(\mathbf{r},\hat{\mathbf{s}}) = -I_\mathrm{w}(\mathbf{r},\hat{\mathbf{s}}) \tag{5}$$

where τ_s is the optical coordinate $(\mathrm{d}\tau_\mathrm{s}=\beta\mathrm{d}s)$. And the contribution to the remainder intensity, I_m, satisfies the equation

$$\frac{\mathrm{d}I_\mathrm{m}}{\mathrm{d}\tau_\mathrm{s}} = (1-\omega)I_\mathrm{b} + \frac{\omega}{4\pi}(G_\mathrm{w}+G_\mathrm{m}) - I_\mathrm{m} \tag{6}$$

where G_w and G_m are components of incident radiation corresponding to wall and medium related intensities and can be expressed as

$$G_\mathrm{w} = \int_{4\pi} I_\mathrm{w}d\Omega \quad \text{and} \quad G_\mathrm{m} = \int_{4\pi} I_\mathrm{m}d\Omega \tag{7}$$

Equations (5) and (6) are subject to the boundary conditions

$$I_\mathrm{w} = \frac{1}{\pi}J_\mathrm{ww} \quad \text{and} \quad I_\mathrm{m} = \frac{1}{\pi}J_\mathrm{wm} \tag{8}$$

respectively, where J_ww and J_wm are contributions of radiosities to wall and medium related intensities, such that

$$J_\mathrm{w} = J_\mathrm{ww} + J_\mathrm{wm} \tag{9}$$

Up to this point, the formulations are identical for both the MDA and the ADA. The difference between the ADA and the MDA approaches lies in the boundary conditions. In the MDA, the entire wall emission is added to the wall-related intensity [1], while for the ADA the blackbody emissive power at the wall is broken up into two pieces

$$E_\mathrm{bw} = E_\mathrm{bwm} + E_\mathrm{bww} \tag{10}$$

such that

$$\begin{aligned} J_\mathrm{wm} &= E_\mathrm{bwm} - \frac{1-\epsilon}{\epsilon}\mathbf{q}_\mathrm{wm}\cdot\hat{\mathbf{n}} \\ J_\mathrm{ww} &= E_\mathrm{bww} - \frac{1-\epsilon}{\epsilon}\mathbf{q}_\mathrm{ww}\cdot\hat{\mathbf{n}} \end{aligned} \tag{11}$$

where q_wm and q_ww are heat flux at wall related to medium related intensity and wall related intensity, respectively. The variable E_bwm constitutes an additional unknown everywhere along the boundary, and a closure for the E_bwm is needed in the ADA. Note that (1) it is possible to have $E_\mathrm{bwm}<0$ if $E_\mathrm{bww}>E_\mathrm{bw}$ or $E_\mathrm{bww}<0$ if $E_\mathrm{bwm}>E_\mathrm{bw}$; (2) E_bww or E_bwm alone are not equal to any emission term but only when summed together, the sum is equal to black body emission related to wall. MDA the intensity related to medium emission leaving a wall, $I_\mathrm{out}=(1/\pi)J_\mathrm{wm}$ is diffuse in

nature and hence constant in all directions. On the other hand, the incoming intensity (using the P_N approximations) from the medium to the wall is directionally variable. This produces a discontinuity in intensity in the direction parallel to the wall, which cannot be followed by the series of spherical harmonics in the ODA and the MDA approaches. In the ADA, the closure for the E_{bwm} is obtained by minimizing the directional discontinuity of the medium-related intensity at the boundary by setting

$$I_{\text{out}} = \frac{1}{\pi} J_{\text{wm}} = I_{\text{in,tan}} \tag{12}$$

where $I_{\text{in,tan}}$ is the incoming intensity related to the medium in the direction tangential to the boundary, i.e., at a polar angle $\theta = \pi/2$ and averaged over all azimuthal directions. For a diffuse surface, the outgoing intensity must be independent of azimuthal angle and thus, Eq. (12) can only be satisfied in an integral sense. Applying the P_N approximation to I_{m}, $I_{\text{in,tan}}$ in Eq. (12) can be written as

$$\begin{aligned}\frac{1}{\pi} J_{\text{wm}} = I_{\text{in,tan}} &= \frac{1}{2\pi}\int_{2\pi} I_{\text{m}}\left(\theta = \frac{\pi}{2}, \psi\right) \mathrm{d}\psi \\ &= \frac{1}{2\pi}\int_{2\pi} \sum_{i=0}^{N} \sum_{m=-i}^{+i} \bar{I}_i^m \bar{Y}_i^m \left(\frac{\pi}{2}, \psi\right) \mathrm{d}\psi = \sum_{i=0}^{N} \bar{I}_i^0 \bar{Y}_i^0 \left(\frac{\pi}{2}\right) \\ &= \sum_{i=0}^{N} \bar{I}_i^0 P_i^0 (\cos\theta = 0) = I_0 - \frac{1}{2}\overline{I}_2^0 + \frac{3}{8}\overline{I}_4^0 \cdots \end{aligned} \tag{13}$$

where ψ is the azimuthal angle, $\bar{I}_i^m$ are the position-dependent intensity coefficients, $\bar{Y}_i^m$ the spherical harmonics, expressed in local coordinates [17], and P_i^0 the associated Legendre polynomials, the last term being $\bar{I}_{N-1}^0$ for a P_N approximation. Note that for the P_1 approximation this criterion leads to full continuity of intensity at the boundary.

Now the P_N approximation needs to be applied to Eq. (6) and boundary condition (8) for the solution of the RTE. As an example, we next outline the solution methodology for the case when the P_1 approximation is applied to Eqs. (6), (8), and (13). For P_1 approximations

$$I_{\text{m}} \approx \frac{1}{4\pi}\left[G_{\text{m}}(\mathbf{r}) + 3\mathbf{q}_{\text{m}}(\mathbf{r}) \cdot \hat{\mathbf{s}}\right] \tag{14}$$

The RTE (6) can then be transformed to [1]

$$\nabla_\tau^2 G_{\text{m}} = -3\nabla_\tau \cdot \mathbf{q}_{\mathbf{m}} = -3[(1-\omega)(4E_{\text{b}} - G_{\text{m}}) + \omega G_{\text{w}}] \tag{15}$$

Using Eqs. (6) and (11), G_{w} can be calculated in terms of unknown E_{bwm}. The boundary condition for the P_1 approximation can be written as [1]

$$-\frac{2}{3}\left(\frac{2-\epsilon}{\epsilon}\right)\hat{\mathbf{n}} \cdot \nabla_\tau G_{\text{m}} + G_{\text{m}} = 4E_{\text{bwm}} \tag{16}$$

Now from Eq. (13), for P_1 approximations

$$\frac{1}{\pi} J_{\text{wm}} = I_0 = \frac{G_{\text{m}}}{4\pi} \tag{17}$$

and, hence, using Eq. (11)

$$\begin{aligned} G_{\text{m}} = 4\pi I_0 = 4J_{\text{wm}} &= 4E_{\text{bwm}} - 4\left(\frac{1-\epsilon}{\epsilon}\right)\mathbf{q}_{\text{wm}} \cdot \hat{\mathbf{n}} \\ &= 4E_{\text{bwm}} - 4\left(\frac{1-\epsilon}{\epsilon}\right)\left(-\frac{1}{3}\nabla_\tau G_{\text{m}}\right) \cdot \hat{\mathbf{n}} \end{aligned} \tag{18}$$

Comparing Eqs. (16) and (18)

$$\nabla_\tau G_{\text{m}} = 0 \quad \text{for all} \quad \epsilon \tag{19}$$

and, thus, also

$$4E_{\text{bwm}} = G_{\text{m}} \tag{20}$$

Note that Eq. (19) (i) allows a certain solution plus an arbitrary constant and (ii) requires that the integral over the sources in Eq. (15), i.e., E_{b} and G_{w} must be zero else the solution becomes transient. Equation (15) can be solved with boundary conditions (19) and (20). For a system of N computational cells, this results in N simultaneous equations similar to the ODA and the MDA, except that the coefficient matrix has a number of additional terms (the G_{m} at wall nodes). Finally, the total value of incident radiation is given by

$$G = G_{\text{m}} + G_{\text{w}} \tag{21}$$

and the total heat flux can be written as

$$\mathbf{q} = \mathbf{q}_{\text{m}} + \mathbf{q}_{\text{w}} \tag{22}$$

where

$$\mathbf{q}_{\text{w}} = \int_{4\pi} I_{\text{w}}(\mathbf{r}, \hat{\mathbf{s}})\hat{\mathbf{s}} d\Omega \quad \text{and} \quad \mathbf{q}_{\text{m}} = \int_{4\pi} I_{\text{m}}(\mathbf{r}, \hat{\mathbf{s}})\hat{\mathbf{s}} d\Omega \tag{23}$$

Sample Calculations

Several one- and two-dimensional radiative heat transfer problems have been investigated, employing the ADAs developed in this study. First, the new ADA method is tested for a 1D slab and concentric spheres with an emitting–absorbing medium enclosed between hot black walls. Results from the ADA method are compared with the ODA, the MDA and also with the exact analytical solutions. A purely isotropically scattering medium confined in a rectangular enclosure is also studied, and the results from the ADA method are compared with those obtained from the MDA, the ODA, and the Monte Carlo simulations. For all the differential approximation based calculations, results from only the P_1 method are shown in this paper; however, the ADA approach can be easily applied to higher-order P_N methods, which will be discussed in a follow-up paper.

1D Problems. Two different 1D slab problems are considered. The first one is a 1D gray, emitting–absorbing, nonscattering slab between two isothermal black plates, both at temperature T_{w}. The medium has a refractive index $n = 1$ and is isothermal at temperature T_{m}. The radiative heat flux between the plates is calculated using the ordinary P_1, the modified P_1, and the advanced P_1 methods and is compared with exact solutions. Details of this problem and solution by the ordinary P_1, the modified P_1, and the analytical method can be found in Modest [1]. As shown by Modest [1], the ordinary P_1 method goes to the correct optically thin limit, but not to correct optically thick limit (since as a result of the temperature step at the wall, there will be always intensity discontinuity at the wall). This problem also illustrates the weakness of the modified P_1 method: while the heat flux goes to the correct optically thin limit, for the optically thick limit the term due to medium emission goes to the value predicted by the ordinary P_1 method, which fails to accommodate the temperature jump and, hence, inhomogeneous intensity distributions. Thus, results for this configuration by the modified P_1 method will lie between exact and ordinary P_1 results, depending on the values on medium and wall temperature. When this problem is solved using the new advanced P_1 method, the solution matches exactly with the analytical expression.

In the second problem, we consider a 1D, gray, absorbing–emitting and isotropically scattering slab with refractive index $n=1$ at radiative equilibrium, contained between two isothermal black walls at temperature T_1 and T_2, respectively. The radiative heat flux between the plates is calculated using various methods similar to the previous case. Details of this problem can be found in Modest [1]. The nondimensional heat flux obtained from the various methods is tabulated in Table 1.

As seen from Table 1, for optically thin and thick limits both the MDA and the ADA perform similarly; for the optically thin case ($\tau_L=0.1$), the error incurred by both these methods is 0.03% compared to the analytical solution while for the optically thick case the error increases to 1.3%. For optically intermediate cases, the MDA method performs slightly better compared to the ADA method. The new ADA method yields slightly better accuracy for optically thin case than the MDA method. For all optically thin and intermediate cases, both the MDA and the ADA show much improvement over the ODA results, while converging to the ODA values for optically thick media. For same optical thicknesses as tabulated in Table 1, the maximum error incurred by the MDA method is 2.1% whereas for the ADA method 1.6% compared to exact solution. The fact that MDA and ADA yield very similar accuracy for 1D test cases leads to the conclusion that separation of wall emission from medium emission offers most of the accuracy improvement for 1D cases; homogenization of intensity distribution at boundaries offers relatively smaller impact on accuracy improvement for very simple 1D test cases.

2D Problem. Sample calculations of 2D heat transfer in a rectangular enclosure have been performed using ordinary, modified, and advanced P_1 approximations. A commercial finite element PDE solver, FlexPDE [18] has been used for all P_1 calculations.

Figure 1 shows a square enclosure with four black walls, in which only the midsection d_h of the bottom wall is hot (at T_h), while the remainder of the bottom wall and the entire other three walls are cold [17]. A gray, homogeneous, and purely isotropically scattering medium ($\sigma_s L=\tau_L$) is considered within the enclosure. Using various methods mentioned above, the dimensionless local irradiation $H/\sigma T^4$ is evaluated along the surface as indicated by the gray shading in Fig. 1 where H is the incoming radiation to the wall boundary. The equations of the ordinary, modified, and advanced P_1 approximations were solved on a total 525 nodes and 242 finite element cells. Typical computation time on a 3.0 GHz Intel Xeon machine for both the ordinary and modified P_1 approximations was <1 s irrespective of the optical thickness. If FlexPDE is employed, the solution to the ADA must be found iteratively, because this code makes no allowance for a thermal source with boundary value dependence. The solution algorithm used for FlexPDE is as follows:

(1) The term G_w is evaluated using a FORTRAN code with initial guess $E_{bwm}=0$.
(2) The result from the FORTRAN code is supplied as an input to FlexPDE to solve for G_m in Eq. (15), with boundary condition (19).
(3) The most recent solution of G_m is used to update E_{bwm} using Eq. (18).
(4) The entire process is repeated until convergence is achieved.

Table 1 Nondimensional radiative heat flux for radiative equilibrium between parallel black plates > $\Psi = q/n^2\sigma(T_1^4 - T_2^4)$

τ_L	ODA	MDA	ADA	Analytical
0.0	1.0	1.0	1.0	1.0
0.1	0.9302	0.9160	0.9160	0.9157
0.5	0.7273	0.7082	0.7085	0.7040
1.0	0.5714	0.5603	0.5612	0.5532
5.0	0.2105	0.2105	0.2105	0.2077

The modified P_1 results were provided as the initial conditions to G_m for the advanced P_1 equations. This led to extremely fast convergence of the advanced P_1 requiring a maximum of 11 iterations.

Figures 2–4 show the results when $d_h=L$, i.e., the entire bottom wall is heated and the medium changes from optically thin ($\tau_L=0.1$) to thick ($\tau_L=5.0$). In all three figures, frame (*a*) shows the flux along the top wall, frame (*b*) along the side wall, and frame (*c*) along the bottom wall, as indicated in Fig. 1 in shaded lines. In addition to the various P_1 based results, Monte Carlo simulation results are also included for comparison. The Monte Carlo results serve as an "exact" solution to this problem.

It can be seen in Figs. 2–4, that the ordinary P_1 approximation yields very inaccurate prediction of irradiation on the surfaces unless the medium is optically thick, because the lower order series of the spherical harmonics cannot correctly capture the strong directional inhomogeneity in intensity distributions. The accuracy of the ordinary P_1 method gradually improves from optically thin to optically intermediate and thick cases. The ordinary P_1 approximation fails to predict the irradiation at the bottom surface for all cases due to intensity discontinuity in the incoming and outgoing directions. For the optically thin case, this leads to nonphysical negative irradiation at the heated bottom wall. For the optically thick case, the ordinary P_1 approximation yields the best accuracy by capturing the shape of the solution somewhat closely.

Substantial improvement can be seen when the MDA approach is applied, because the medium generated intensity is almost isotropic. For all cases, the modified P_1 method predicts surface irradiation accurately, except for the optically intermediate case where the irradiation on the bottom wall is predicted somewhat inaccurately.

Application of the new ADA approach to the P_1 approximation results in the best accuracy. For all cases, the advanced P_1 approximation results almost fall on top of the exact Monte Carlo results. Since this method makes the intensity distribution for the P_1 approximation exactly homogeneous at the boundaries, the advanced P_1 method yields better accuracy than the modified P_1 approximation for all cases, noticeably for the bottom wall in the optically intermediate case, where the MDA incurs inaccuracy.

A more severe test case is considered next by setting $d_h/L=0.2$, i.e., only a small portion of the bottom surface is heated. This will cause even more intensity inhomogeneities along the bottom surface. Figures 5–7 show the results for optically thin ($\tau_L=0.1$) to thick ($\tau_L=5.0$) cases, similar as before. As in the previous case, ordinary P_1 cannot predict the surface irradiation very well on all surfaces for the optically thin media, particularly the bottom surface, showing nonphysical behavior across the heated strip.

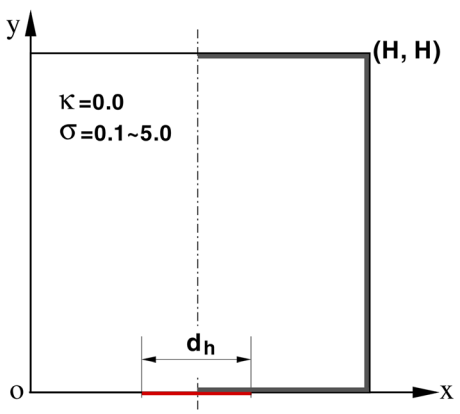

Fig. 1 Schematic diagram of a rectangular enclosure containing scattering medium with hot strip at the bottom center

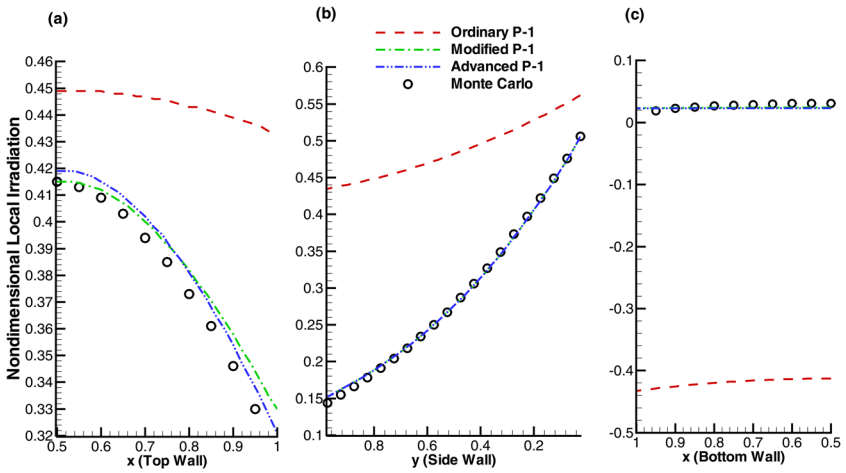

Fig. 2 Comparison of nondimensional irradiation on surfaces, full bottom surface heated, optically thin case, $\tau_L = 0.1$

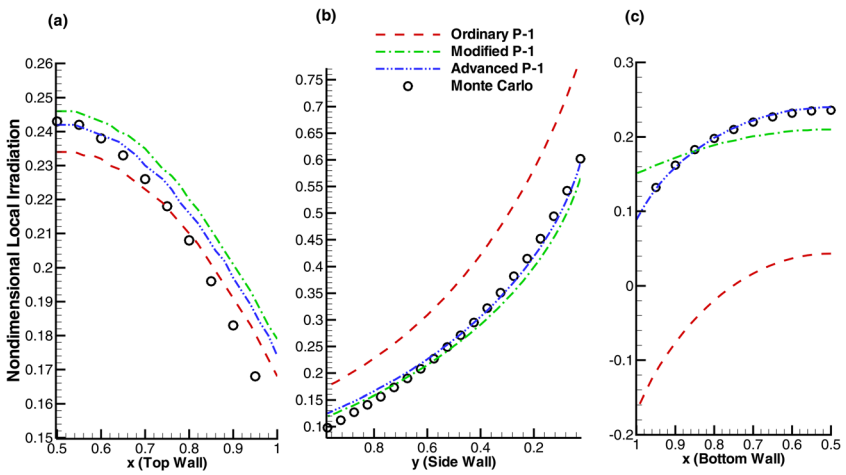

Fig. 3 Comparison of nondimensional irradiation on surfaces, full bottom surface heated, optically intermediate case, $\tau_L = 1.0$

The modified P_1 approximation gives excellent accuracy for these cases also, except for the bottom wall in optically thin and intermediate cases. For these two cases, the directional gradient of intensity distribution near the bottom wall is very severe and the modified P_1 is incapable of accommodating such sharp gradients. The advanced P_1 method yields better accuracy for all cases, including predicting the irradiation on the bottom surface for the optically thin and intermediate cases. Since the advanced

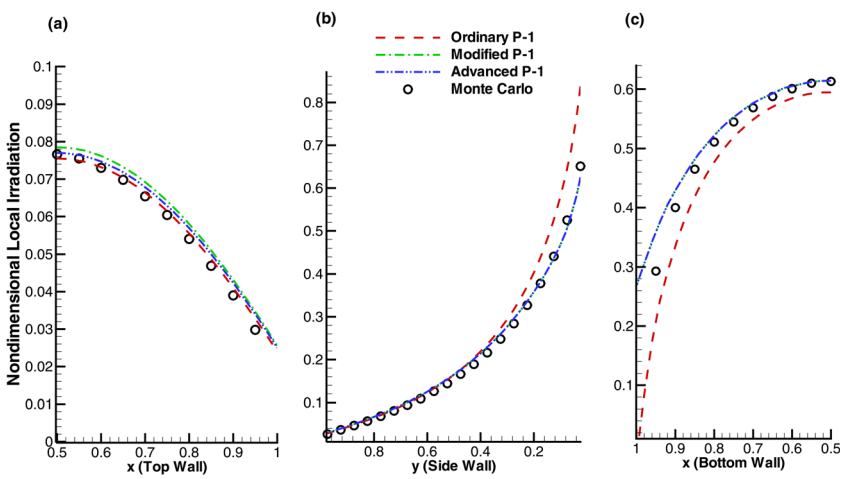

Fig. 4 Comparison of nondimensional irradiation on surfaces, full bottom surface heated, optically thick case, $\tau_L = 5.0$

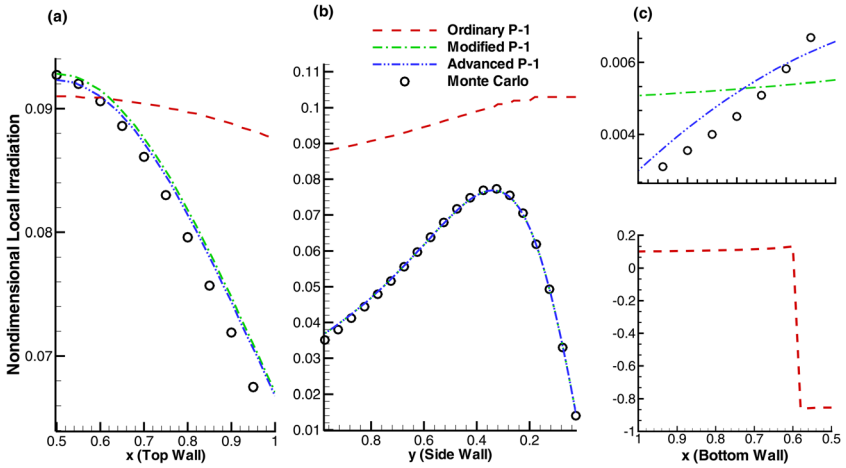

Fig. 5 Comparison of nondimensional irradiation on surfaces, strip of the bottom surface heated, optically thin case, $\tau_L = 0.1$

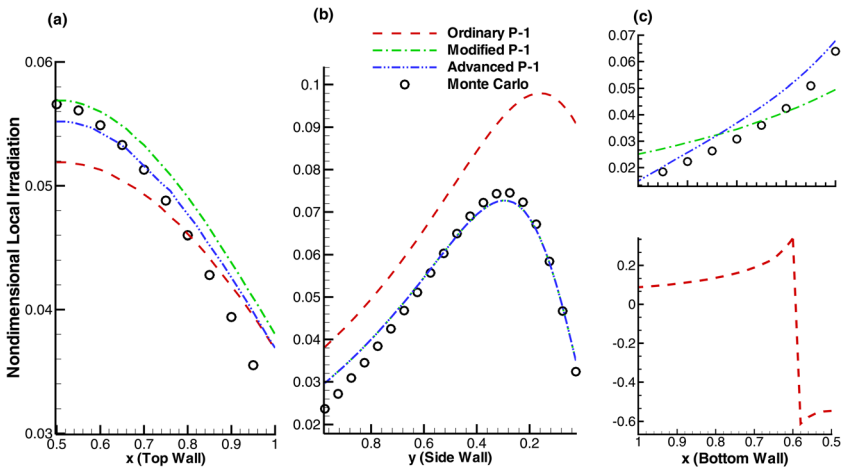

Fig. 6 Comparison of nondimensional irradiation on surfaces, strip of the bottom surface heated, optically intermediate case, $\tau_L = 1.0$

P_1 approach makes the intensity distribution perfectly homogeneous for the P_1 method, it is capable of handling such severe problems successfully. The accuracy of the advanced P_1 method is found to improve from the optically thin case to the optically thick case. However, none of the P_1 approximations (ordinary, modified, and advanced)-based results exactly replicates the Monte Carlo solutions. Hence, the ADA approach should be applied to the higher-order P_N approximations (which the ADA method is capable of) if better accuracy is desired.

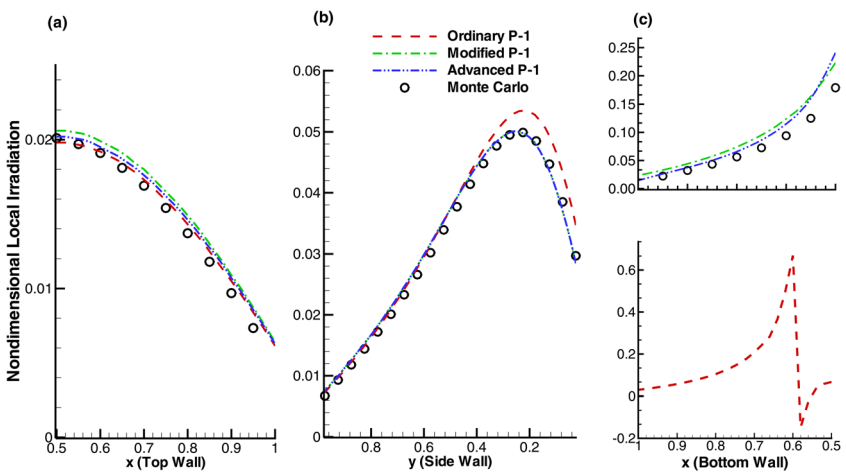

Fig. 7 Comparison of nondimensional irradiation on surfaces, strip of the bottom surface heated, optically thick case, $\tau_L = 5.0$

Conclusion

A novel approach, termed here as ADA was developed and discussed in this article. The ADA approach was developed to alleviate the inaccuracies incurred by the P_N approximations due to intensity discontinuities at the boundaries. The overall intensity is broken up into two parts—one is related to the wall emission and the other to a combination of wall and medium emission. At the wall, the directional gradient of the intensity related to the medium emission is minimized through the boundary conditions. This paper outlines the detailed development of the ADA with discussion of differences between the ADA and a previous modification of P_N approximation, i.e., the MDAs. Sample radiation calculations were performed for a 1D slab, and concentric spheres, and 2D media. Although the computational cost for the ADA is larger compared to the ODA or MDA, the ADA is capable of completely accommodating sharp gradients in intensity distributions between boundary wall and medium interface and hence removes the inherent cause of inaccuracy in any P_N approximation. For cases with extreme intensity inhomogeneity between boundary and medium interface, the new ADA method yields excellent accuracy compared to the MDA.

Acknowledgment

The model presented here was developed during the period when the senior author (mfm) was at the University of Karlsruhe, Germany in the framework of a Humboldt Research Award. The authors acknowledge the support provided by both the University of Karlsruhe and the Alexander von Humboldt Foundation.

Nomenclature

E_b = blackbody emission
G = incoming radiation
H = incoming radiation to wall boundary
I = radiative intensity
I_b = blackbody intensity
I_m^i = position dependant intensity coefficient
J = total surface radiosity
L = geometric length
$\hat{n}$ = surface normal
P_i^0 = associated Legendre polynomials
q = radiative heat flux
$\mathbf{r}$ = position vector
s = distance along path
$\hat{s}$ = unit direction vector
T = temperature
Y_m^i = spherical harmonics in local coordinates

Greek Symbols

β = extinction coefficient
ϵ = surface emittance
θ = polar angle
κ = absorption coefficient
σ = Stefan–Boltzmann constant = 5.67×10^{-8} W/m^2 K^4
σ_s = scattering coefficient
τ_s = optical thickness along path s
Φ = scattering phase function
ψ = azimuthal angle
ω = scattering albedo
Ω = solid angle

Subscripts

b = blackbody emission
i = index of terms in P_N approximation
m = medium
w = wall

References

[1] Modest, M. F., 2003, *Radiative Heat Transfer*, 2nd ed., Academic Press, New York.
[2] Chai, J. C., Lee, H. S., and Patankar, S. V., 1993, "Ray Effect and False Scattering in the Discrete Ordinates Method," Numer. Heat Transfer, Part B, **24**(2), pp. 373–389.
[3] Kofink, W., 1959, "Complete Spherical Harmonics Solution of the Boltzmann Equation for Neutron Transport in Homogeneous Media With Cylindrical Geometry," Nucl. Sci. Eng., **6**, pp. 473–486.
[4] Bayazitoğlu, Y., and Higenyi, J., 1979, "The Higher-Order Differential Equations of Radiative Transfer: P_3 Approximation," AIAA J., **17**(4), pp. 424–431.
[5] Mengüç, M. P., and Viskanta, R., 1985, "Radiative Transfer in Three-Dimensional Rectangular Enclosures Containing Inhomogeneous, Anisotropically Scattering Media," J. Quant. Spectrosc. Radiat. Transfer, **33**(6), pp. 533–549.
[6] Mengüç, M. P., and Viskanta, R., 1986, "Radiative Transfer in Axisymmetric, Finite Cylindrical Enclosures," ASME J. Heat Transfer, **108**(2), pp. 271–276.
[7] Tong, T. W., and Swathi, P. S., 1987, "Radiative Heat Transfer in Emitting–Absorbing–Scattering Spherical Media," J. Thermophys. Heat Transfer, **1**(2), pp. 162–170.
[8] Ou, S. C. S., and Liou, K. N., 1982, "Generalization of the Spherical Harmonic Method to Radiative Transfer in Multi-Dimensional Space," J. Quant. Spectrosc. Radiat. Transfer, **28**(4), pp. 271–288.
[9] Yang, J., and Modest, M. F., 2007, "High-Order *P-N* Approximation for Radiative Transfer in Arbitrary Geometries," J. Quant. Spectrosc. Radiat. Transfer, **104**(2), pp. 217–227.
[10] Olfe, D. B., 1967, "A Modification of the Differential Approximation for Radiative Transfer," AIAA J., **5**(4), pp. 638–643.
[11] Olfe, D. B., 1968, "Application of a Modified Differential Approximation to Radiative Transfer in a Gray Medium Between Concentric Sphere and Cylinders," J. Quant. Spectrosc. Radiat. Transfer, **8**(3), pp. 899–907.
[12] Olfe, D. B., 1970, "Radiative Equilibrium of a Gray Medium Bounded by Nonisothermal Walls," Prog. Astronaut. Aeronaut., **23**, pp. 295–317.
[13] Olfe, D. B., 1973, "Radiative Equilibrium of a Gray Medium in a Rectangular Enclosure," J. Quant. Spectrosc. Radiat. Transfer, **13**(9), pp. 881–895.
[14] Modest, M. F., 1974, "Two-Dimensional Radiative Equilibrium of a Gray Medium in a Plane Layer Bounded by Gray Non-Isothermal Walls," ASME J. Heat Transfer, **96**(4), pp. 483–488.
[15] Modest, M. F., 1975, "Radiative Equilibrium in a Rectangular Enclosure Bounded by Gray Non-Isothermal Walls," J. Quant. Spectrosc. Radiat. Transfer, **15**(6), pp. 445–461.
[16] Modest, M. F., and Stevens, D., 1978, "Two Dimensional Radiative Equilibrium of a Gray Medium Between Concentric Cylinders," J. Quant. Spectrosc. Radiat. Transfer, **19**(3), pp. 353–365.
[17] Modest, M. F., and Yang, J., 2008, "Elliptic PDE Formulation and Boundary Conditions of the Spherical Harmonics Method of Arbitrary Order for General Three-Dimensional Geometries," J. Quant. Spectrosc. Radiat. Transfer, **109**(9), pp. 1641–1666.
[18] FlexPDE Software, PDE Solutions, Inc., Antioch, CA.